Finite-element distributions as an apparatus for detection of the Einstein-Brillouin-Keller quantized energy levels

Piotr Sułkowski[1] and Krzysztof Sokalski[2]
[1]*Institute of Physics, Jagiellonian University, 30-059 Kraków, ul. Reymonta 4, Poland*
[2]*Institute of Computer Science, Technical University of Częstochowa, 42-200 Częstochowa, al. Armii Krajowej 17, Poland*
(Received 20 September 2004; published 12 April 2005)

Regularities encountered for some systems with nongeneric spacing distributions are discussed and a corollary which connects these regularities with the Einstein-Brillouin-Keller (EBK) quantized energy levels is formulated. Properties of quantum systems are investigated with the help of finite elements probability distributions. Analytic properties of three-point finite-element distributions are investigated. Four-point finite-element distributions for an integrable model are presented. Analytic properties of such distributions for chaotic and integrable models are discussed.

DOI: 10.1103/PhysRevE.71.046206 PACS number(s): 05.45.Mt, 05.45.Pq, 42.50.−p

I. INTRODUCTION

The understanding of the connection between spectral properties of classically chaotic systems with a few degrees of freedom and random matrix theory (RMT) was not immediate. The reason was that RMT had been originally developed in nuclear physics and for a long time had been conceived as a statistical approach to spectral fluctuations of complex nuclei, atoms, molecules, etc. [1,2].

The applicability of the RMT predictions for quantum chaos was not fully recognized until Bohigas *et al.* [3] stated the conjecture: "*Spectra of time-reversal invariant systems whose classical analogues are K systems show the same fluctuation properties as predicted by the GOE*." Definintions of Gaussian orthogonal ensemble (GOE) and two other random matrix ensembles GUE, GSE can be found in [1,2]. The *K* systems are classical systems with the strongest mixing. In the same paper, an alternative stronger version of this conjecture was also stated, where *K* systems were replaced by less chaotic ergodic systems. Both forms of this conjecture are referred to as a Bohigas-Giannoni-Schmit conjecture. For other symmetry classes, the GOE is replaced by GUE and GSE, respectively. It is worth noting that this conjecture was stated without a reference to the semiclassical regime, i.e., to the limit $\hbar \to 0$. The universality of Poisson spacing distribution $P(s)=\exp(-s)$, obtained by Berry and Tabor [4] for integrable models may be considered as the analog of the Bohigas-Giannoni-Schmit conjecture in such cases. But, as it will be reviewed in the next section, nearest neighbour spacing (NNS) distributions obtained for systems near to being integrable may be distinctively different from this distribution. Therefore, a question appears whether these distributions have some common features which would distinguish them from those belonging to the chaotic systems. Presented below concepts were formulated on the basis of an observation that significant in the context of quantum integrability are smoothness classes of spacing distributions.

II. SOME SYSTEMS WITH EXCEPTIONAL SPACING DISTRIBUTIONS

Since the publication of the paper [4], it has been known that for generic quantum integrable systems Poisson spacing distribution can be derived. It is possible to expect that spacing distributions, obtained for systems for which some remnants of integrability will preserve should share some common features with Poissonian distribution. Below we will present some of such systems paying special attention to discontinuities of their spacing distributions. After this review has been completed, we would formulate an appropriate corollary, linking this specific feature of spacing distributions with one aspect of quantum integrability. We begin our discussion with the most popular quantum systems.

Harmonic oscillators

In the paper [5] it has been shown that for these systems, whose integrability is rather obvious, a phenomenon of the nonexistence of spacing distributions or, in other words, nonconvergence of spacing histograms appears. For oscillators with commensurable frequencies having f degrees of freedom, the level density takes the form

$$\rho(U)=\sum_{l=0}^{\infty} a_l \delta(U-(l^f/f!)), \tag{1}$$

where a_l is equal to the number of permutations of f nonnegative integers whose sum is l. The leading term for large l, which underestimates its true value is

$$a_l \to l^{f-1}/(f-1)! \text{ as } l \to \infty. \tag{2}$$

The level density formula (1) shows no signs of stochasticity and the spacing distributions obtained for a particular number of energy levels are composed of a separate Dirac's delta functions. Spacing distributions obtained for two two-dimensional harmonic oscillators having incommensurate frequencies are presented in Figs. 1(a) and 1(b). There can be observed strong oscillations and discontinuities of histograms. These examples are representative of the whole class of oscillators with incommensurate frequencies.

Systems with mixed phase space

In 1984 Berry and Robnik [6] calculated semiclassical limiting level spacing distributions for systems whose clas-

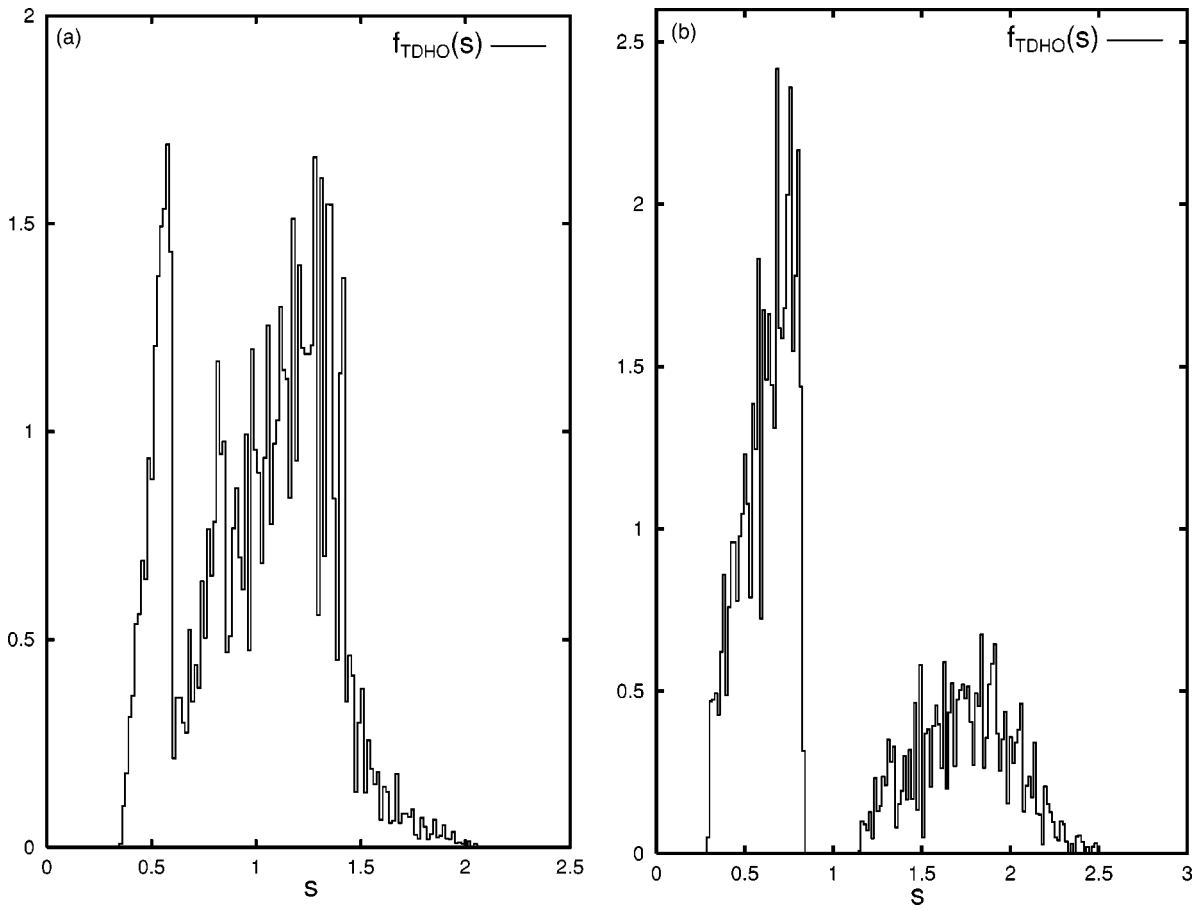

FIG. 1. Level spacing distributions $f_{\mathrm{TDHO}}(\mathrm{s})$ for two-dimensional harmonic oscillators with frequency ratio α. (a) $\alpha=1/\sqrt{2}$, (b) $\alpha=1/\sqrt{7}$. For both figures 50 000 levels from 75 000 level were processed.

sical energy surface was divided into separate regions in which motion was regular or chaotic. There was made an assumption that the spectrum was a superposition of the statistically independent sequences of levels from each of the classical phase-space regions. Sequences from regular regions were proposed to have the Poisson spacing distributions, and for the ones from irregular regions spacing distributions were given by the Wigner surmise (i.e., GOE spacing distribution approximation cf. [2]). While performing the superposition of level sequences, it was assumed that there were N sequences of levels with mean densities ρ_i proportional to Liouville measures of appropriate regions. The NNS distribution for the full spectrum was obtained in the form

$$P(s)=\frac{1}{\rho}\frac{d^2}{ds^2}\left[e^{-\rho_1 s}\prod_{i=2}^{N}\mathrm{erfc}\left(\frac{\sqrt{\pi}}{2}\rho_i s\right)\right], \tag{3}$$

where

$$\mathrm{erfc}(x)\equiv(2/\sqrt{\pi})\int_x^\infty dt\, e^{-t^2}$$

and $\rho=\Sigma_{i=1}^{N}\rho_i$. For systems with three or more degrees of freedom f, Arnold diffusion ensures that there is just one chaotic region forming a connected web, whereas when $f=2$ there are, generically, infinitely many chaotic regions [7]. In such cases, it is expected that, in practice, formula (3) will be applied for finite N, with N being the number of chaotic regions considered to have the significant measure. From the reminded result, it is possible to calculate the value of the spacing distribution at $s=0$ which is

$$\begin{aligned}P(0)&=\rho-\frac{1}{\rho}\sum_{i=2}^{N}\rho_i^2\\&=\rho\left(1-\frac{1}{\rho^2}\sum_{i=2}^{N}\rho_i^2\right)\\&=\rho\left(1-\frac{\sum_{i=2}^{N}\rho_i^2}{(\sum_{i=1}^{N}\rho_i)^2}\right)\geqslant 0.\end{aligned} \tag{4}$$

We interpret this result as similar to the discontinuity of spacing distribution at zero [with the assumption that $P(s)=0$ for $s<0$] which appears in the Poissonian case.

The derivation presented above, from which the nonzero value of spacing distribution at zero was obtained, requires uniform level densities on the considered interval and, therefore, there may appear some questions about its applicability. The assumption that level sequences supported by different regular and irregular regions in the classical phase space are statistically independent, also might not be strictly satisfied.

Indeed, according to the recent results obtained by Podolskiy and Narimanov [8], when the dynamical tunneling is taken into account, the prediction about the nonzero value of spacing distribution at zero no longer holds. As these results are relatively new, it is not entirely clear whether the assumption that "*chaos-assisted tunneling leads to the level repulsion between any two regular levels via an 'intermediate' state*" [8], is always true, we have discussed here inferences which can be drawn from the Berry-Robnik distribution.

The hydrogen atom in the magnetic field

For such an atom, the Hamiltonian in the homogeneous constant magnetic field B in z direction reads

$$H = \frac{\mathbf{p}^2}{2m} - \frac{e^2}{r} - \omega_L L_z + \frac{1}{2}\omega_L^2(x^2+y^2), \tag{5}$$

with $r=\sqrt{x^2+y^2+z^2}$ and where $\omega_L = eB/2mc$ is the Larmor frequency. With increasing magnetic field strength it also increases the volume of classical's phase space chaotic parts. When the magnetic field is expressed in natural units, the system is described in the rotating frame with the frequency equal to Larmor frequency ω_L, and in cylindrical coordinates $(\rho=\sqrt{x^2+y^2}, z)$, then for fixed M values, the Hamiltonian reads [9]

$$H = \frac{1}{2}(p_\rho^2 + p_z^2) + \frac{M^2}{2\rho^2} - \frac{1}{\sqrt{\rho^2+z^2}} + \frac{1}{8}\gamma^2\rho^2, \tag{6}$$

where p_ρ and p_z are momenta in ρ and z directions while γ is proportional to the magnetic field B. The Hamiltonian (6) has the scaling property $H(\mathbf{p},\mathbf{r},\gamma)=\gamma^{2/3}H(\gamma^{-1/3}\mathbf{p},\gamma^{2/3}\mathbf{r},1)$. Therefore, all properties of this system depend only on the scaled energy $\epsilon=\gamma^{-2/3}E$. The spacing distribution for $\epsilon \geqslant -0.12$ is similar to GOE distribution. The reason for this similarity is that, in spite of the fact that the Hamiltonian (5) is not invariant under time reversal, it is invariant under the product of a reflection about any axis perpendicular to the z axis and the time-reversal operator. Zakrzewski *et al.* [9] made the following observation. Being very close to the ionization threshold, the nearest-neighbor spacing distribution deviates from the Wigner surmise as is shown in Figs. 2(a) and 2(b). This is caused by an almost complete absence of spacings larger than about 1.7 mean level spacings, whose effect is also responsible for the discontinuity of spacing distribution at this point. The underlying reason for such behavior is that although classical motion is chaotic here, the diamagnetic term in Eq. (6) confines the motion only in the (x,y) plane. In the z direction, the electron can move very far away from the proton. At so large distances, the Hamiltonian is the sum of two integrable parts

$$H \simeq H_{\text{sep}} = H_z + H_\rho = \frac{p_z^2}{2} - \frac{1}{|z|} - \frac{p_\rho^2}{2} - \frac{\gamma^2\rho^2}{8}, \quad \text{when } |z| \gg \rho. \tag{7}$$

It has also been shown in [9] that this effect can also be described by a regular Hamiltonian coupled to a chaotic one modeled by a random matrix.

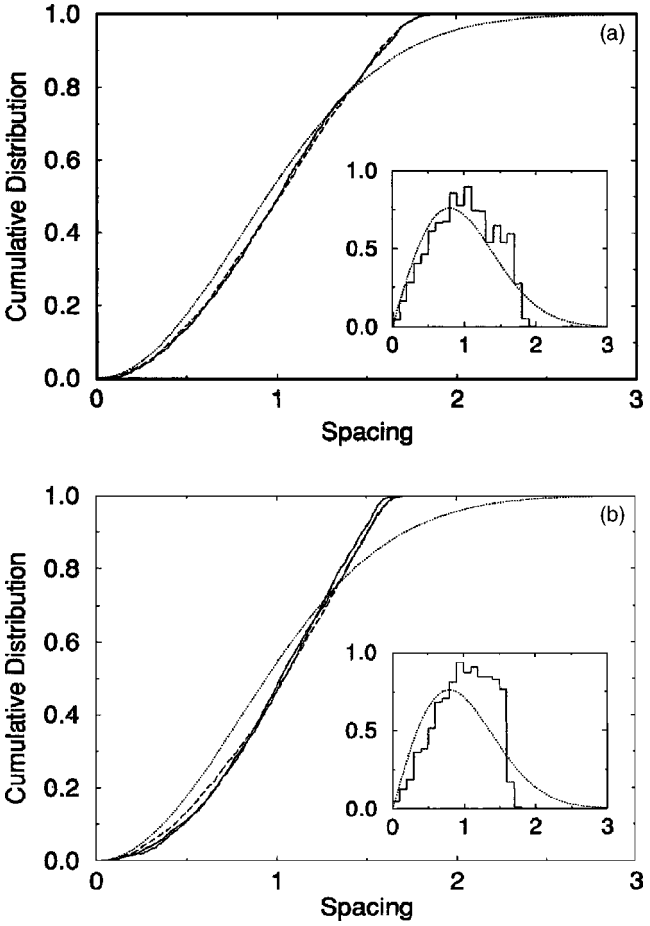

FIG. 2. Cumulative nearest spacing distributions for hydrogen atom in magnetic field, in insets spacing distributions themselves. Levels near ionization threshold are considered. In (a) from interval $[-0.4\gamma;-0.3\gamma]$; in (b) from interval $[-0.2\gamma;-0.1\gamma]$. [Figures reprinted with permission from J. Zakrzewski, K. Dupret, and D. Delande, Phys. Rev. Lett. **74**, 522 (1995). ©1995 by the American Physical Society].

Quartic oscillator

This system defined by the following Hamiltonian

$$H = \frac{p_x^2+p_y^2}{2} + \frac{x^2y^2}{2} + \frac{\beta(x^4+y^4)}{4} \tag{8}$$

was also analyzed in the manner which was interesting for us in the Ref. [9]. According to [10,11] and references therein, the classical motion of this system is chaotic in the limit $\beta \to 0$. The spacing distributions for the states of this system which are symmetric and antisymmetric with respect to the x and y axes are replotted in Figs. 3(a) and 3(b), respectively (the parameter β was taken equal to zero). Also, in the case of this system, the lack of large spacings can be observed, which manifests itself as a discontinuity of a spacing distribution; cf. Fig. 3(a). The occurrence of such an effect can be explained by the adiabatic separation of variables in the neighborhood of a certain *channel orbit*, which is defined as an adiabatic well. In such a case, some energies of the sys-

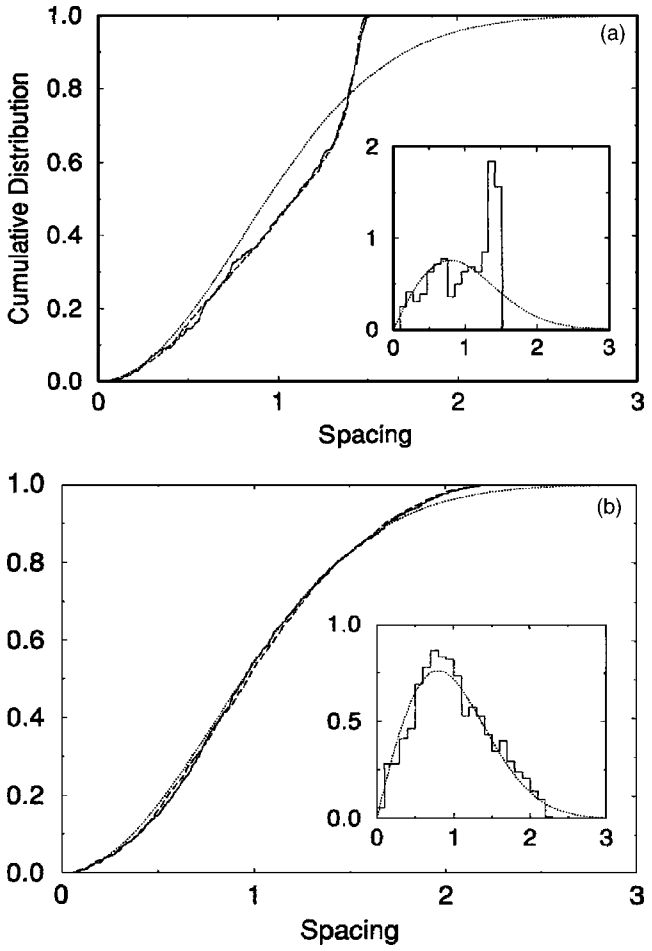

FIG. 3. Cumulative nearest neighbor spacing distributions for the quartic oscillator. In insets the pacing distributions. On the left are shown series of states symmetric with respect to the x and y axes. On the right there are shown series of states antisymmetric with respect to the x and y axes. [Figures reprinted with permission from J. Zakrzewski, K. Dupret and D. Delande, Phys. Rev. Lett. **74**, 522 (1995). ©1995 by the American Physical Society].

tem are given by the local adiabatic Hamiltonian, which is integrable [11]

$$\epsilon_{n,m} = H(S_{\|} = m + \alpha_{\|}/4, \quad S_{\perp} = n + \alpha_{\perp}/4), \tag{9}$$

in formula (9) $S_{\perp}$ and $S_{\|}$ are action components respectively perpendicular and parallel to the channel orbit and $\alpha_{\|}$ and $\alpha_{\perp}$ are relevant Maslov indices and $\beta = 0.01$. Therefore, the eigenenergies may be written as

$$\epsilon_{n,m} = (-a/b)(m + \alpha_{\|}/4) + (n + \alpha_{\perp}/4)/b, \tag{10}$$

reducing part of the system spectrum to the spectrum of the two dimensional harmonic oscillator. The reliability of such an approximation, which in fact predicts presence of the EBK quantized levels in the spectrum of this system may be checked in Tables I and II of Ref. [11] which contain comparison of eigenenergies numerically computed and obtained by means of adiabatic Hamiltonian (10). It should be noticed, however, that from the analysis of Fig. 3(b) it is possible to conclude that to obtain significant discrepancies between

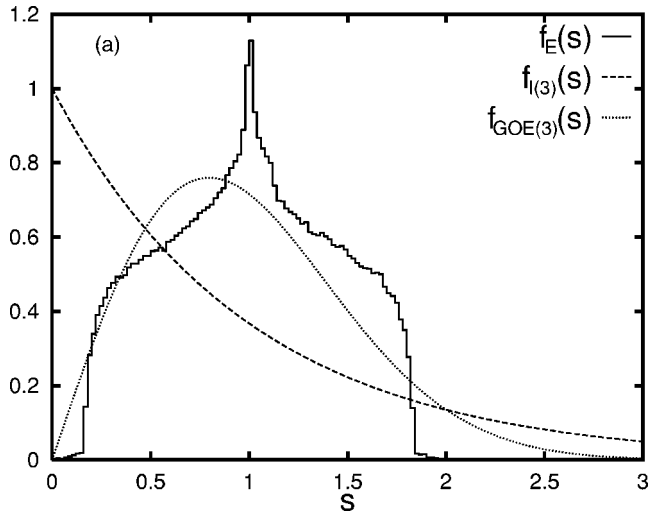

FIG. 4. The probability density distribution of the dimensionless spacing $f_E(s)$ for one-dimensional box with spin dependent sizes, there are also presented analytically predicted probability distributions for I(3) model (dashed line) and GOE(3) (dotted line). Appropriate models are defined in Sec. III and in [13] (plot taken from [13]).

RMT predictions and experimental data the density of regular levels cannot be arbitrarily small.

One-dimensional box with spin state dependent size

A strange spacing probability distribution plotted in Fig. 4 had been found in a system introduced by Ruijgrok and Sokalski [12] and was further investigated by Sułkowski and Sokalski [13]. This system consists of a particle which possesses half integer total angular momentum. The particle is subjected to a constant magnetic field and moves in a one-dimensional box with hard walls. It is changing its properties (e.g., linear dimension) as a result of the coupling between the magnetic field and angular momentum, therefore one may think of it as of the paramagnetic atom. On the other hand, it could be assumed that the box extends from $-a$ to a when the atom is in the state $|\frac{1}{2},\frac{1}{2}\rangle$ and from $-b$ to b when it is in the state $|\frac{1}{2},-\frac{1}{2}\rangle$. It is also assumed that $b>a$. The Hamiltonian of this system has the form

$$\hat{H} = \hat{p}_y^2 + \kappa^2 \hat{\sigma}_x + V(y), \tag{11}$$

with

$$V(y) = 0.5\{[V_1(y) - V_2(y)]\hat{\sigma}_z + [V_1(y) + V_2(y)]\hat{1}_2\},$$

$$V_1(y) = \begin{cases} 0, & \text{if } y < |a|, \\ +\infty, & \text{if } y > |a|, \end{cases}$$

$$V_2(y) = \begin{cases} 0, & \text{if } y < |b|, \\ +\infty, & \text{if } y > |b|, \end{cases}$$

where σ_x and σ_z are Pauli spin matrices. When the spin does not collide with the walls, the equations of motion are integrable, second integral of motion is $\hat{S}_x^H = 1/2\sigma_x^H$ (where H

denotes Heisenberg's picture). Let us now investigate what happens when a collision occurs. Since it is almost instantaneous, we can neglect the precession of the spin around x axis whose rate is given by a Larmor frequency. Then, at the neighborhood of point $y=a$ the Hamiltonian takes the form

$$\hat{H} = \hat{p}_y^2 + 0.5V_1(a)(\hat{\sigma}_z + \hat{1}_2) \tag{12}$$

and it is easy to verify that $\hat{S}_z^H$ becomes the second invariant of motion for this system (analogous analysis may be performed near the second turning point). The spacing distribution obtained by us in [13], is presented in Fig. 4. Despite the fact that classical time evolution of the system is almost entirely integrable, the spacing distribution for this system does not reveal the Poissonian character. Instead, a peak can be observed, which might suggest the existence of a spacing distribution singularity for this system. The procedure which should be performed in order to explicitly show EBK quantized level in the spectrum of this system is similar to the one which will be described in the next paragraph for quantum graphs. This is a case because for the system considered, there are known appropriate secular equations (for symmetric and antisymmetric levels, respectively) [12]. Nevertheless, due to the fact that such procedure in this case is rather involved and relies on some approximations it will be given elsewhere.

Finite quantum graphs

Quantum graphs have recently been the subject of intense studies [14,15]. The graph can be defined as a set of V vertices connected by B bonds. The eigenfunctions of the graph are completely determined by their values at the vertices $\{\varphi_i\}$. At any bond (i,j), the component $\Psi_{i,j}$ can be written as

$$\Psi_{i,j} = \frac{e^{iA_{i,j}x}}{\sin kL_{i,j}}(\varphi_i \sin[k(L_{i,j}-x)] + \varphi_i e^{-iA_{i,j}L_{i,j}} \sin kx), \tag{13}$$

where $A_{i,j}=-A_{j,i}$ is a magnetic vector potential and k is the wave number. The substitution of $\Psi_{i,j}(x)$ given by (13) for $i,j=1,\ldots,V$ into appropriate current conservation conditions leads to a set of linear homogeneous equations for the φ's, which has a nontrivial solution when the determinant of its coefficient's matrix equals zero. This condition leads to a secular equation, which can be solved numerically to provide an arbitrary large sequence of eigenvalues $\{k_n\}$. It occurs that, for quantum graphs, periodic orbits proliferate exponentially with the length of periodic orbit. Therefore, topological entropy, defined as

$$\Lambda = \lim_{l\to\infty} \frac{\ln[N(l)]}{l}, \tag{14}$$

where l is the length of the periodic orbit and $N(l)$ is the total number of orbits of length $\leqslant l$, has a positive value and is approximately equal to an average valency of a vertex. The phase space of such systems is bounded and, therefore, the dynamics of particles is mixing [16]. For some quantum graphs like, for example, for tetrahedron and completely connected pentagon numerically obtained spacing distributions are already known [15]. Distributions obtained for both of these systems are good approximations of GOE predictions for chaotic systems. However, in spite of what might be expected from the considerations concerning topological entropy, this is not a general rule for quantum graphs. This observation may be illustrated by results for the three bond star [cf. Fig. 5(a)] with all bonds having different lengths in Fig. 6(a) and for the circle with diameter [cf. Fig. 5(b)] in Fig. 6(b). In both cases, singularities in the spacing distribution obtained for those systems can be observed.

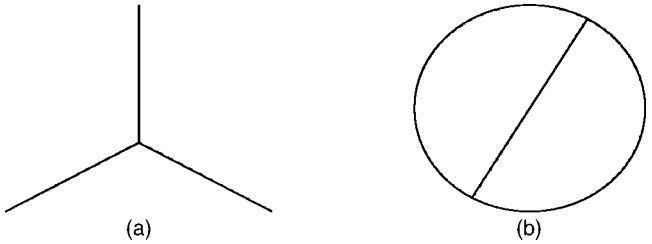

FIG. 5. (a) Three bond star; (b) circle with its diameter.

Moreover, there are, quantum graphs for which, due to their simplicity, it is possible to obtain analytical expressions for spacing distributions. Starting from appropriate spectral equations the authors of work [15] were able to find such formulas for several graphs. Let us begin this short resume with a graph consisting of two loops attached to a single vertex forming an eight shape figure, for which spacing distribution has the form

$$P(\Delta) = \begin{cases} \dfrac{1}{2}, & \text{if } 0 < \Delta < 2, \\ 0, & \text{otherwise}. \end{cases} \tag{15}$$

As another example let us consider a graph composed of a bond and a loop attached to a vertex. For this graph, spacing distribution has the form $P(\Delta)\to l_2/(l_1+l_2)$ when $\Delta\to 0$. Next we would like to present results for the graph having the shape of three-bond star. It was possible to obtain an approximate expression for this graph's spacing distribution in the case when two bonds have equal lengths, for instance $l_3=l_1$. Then, for values of l_1 and l_2 from certain intervals, it is possible to write the spacing distribution as

$$P(\Delta) = 2l_1\left(l_2 + \frac{l_1}{2}\right)L^{-2} + a_0 + \frac{3l_1^4\pi^2}{4L^4}\Delta^2 + O(\Delta^4), \tag{16}$$

where a_0 is a constant. For graphs with disconnected bonds, i.e., those obtained by imposing Dirichlet boundary conditions on the vertices and called sometimes "integrable graphs," the spacing distribution reads

$$P(\Delta) = \sum_{k=1}^{n}\sum_{j\neq k}^{n}\frac{l_k}{L_{\text{tot}}}\frac{l_j}{L_{\text{tot}}}\left[\prod_{i\neq\{j,k\}}^{n}\left(1-\frac{l_i}{L_{\text{tot}}}\Delta\right)\right]\Theta\left(\frac{L_{\text{tot}}}{l_1}-\Delta\right) + \frac{l_1}{L_{\text{tot}}}\left[\prod_{i\neq 1}^{n}\left(1-\frac{l_i}{L_1}\Delta\right)\right]\left(\Delta-\frac{L_{\text{tot}}}{l_1}\right), \tag{17}$$

where l_1 is the largest length of the graph, and $L_{\text{tot}}=\Sigma_{i=1}^{n}l_i$. The Poisson distribution is obtained in the limit $l_1/L_{\text{tot}}\to 0$.

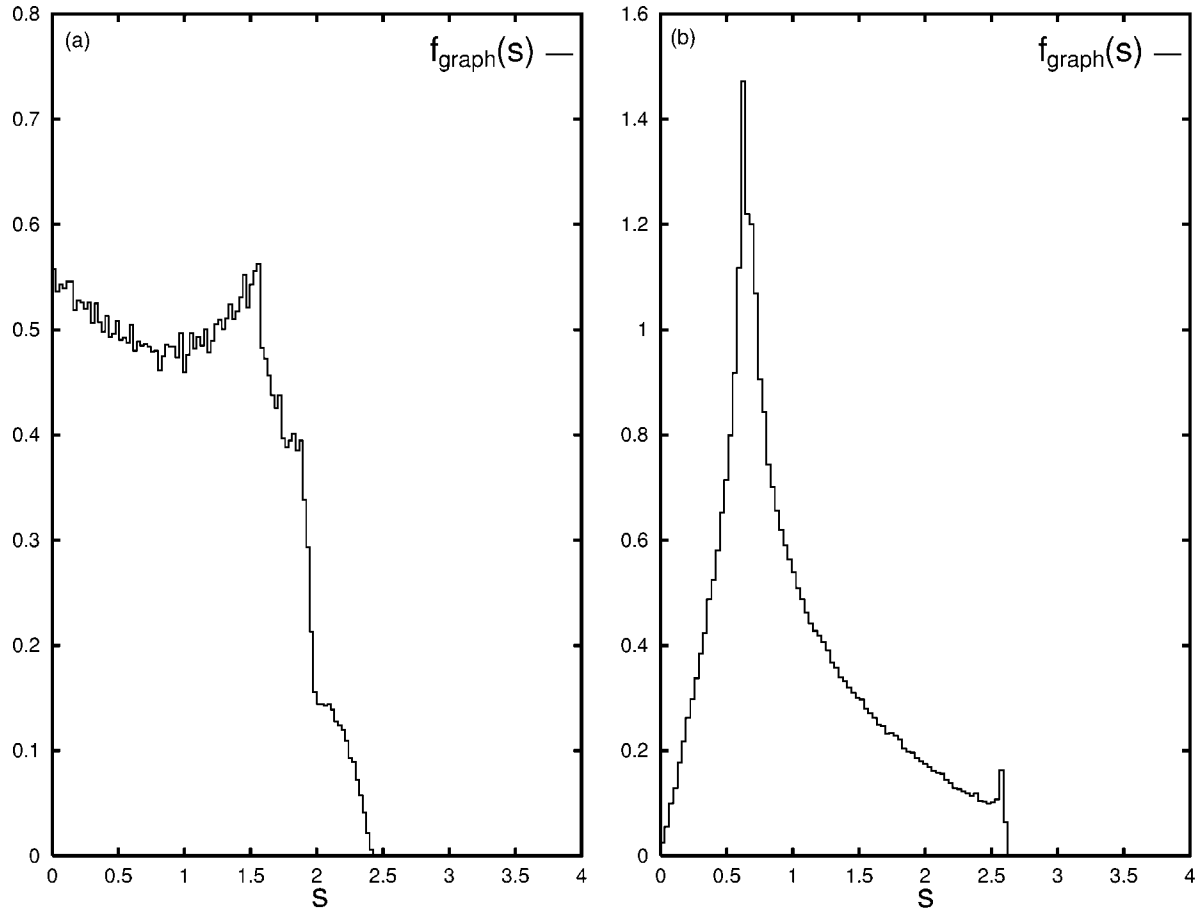

FIG. 6. The probability density distribution of the dimensionless spacing for $f_{\text{graph}}(s)$ for: (a) three bond star, (b) circle with its diameter.

Another distinctive feature of spacing distributions obtained from the formula (17) is the existence of maximum spacing.

Presented results show that, for simple graphs, spacing distributions generally depend on the topology of the considered graph and are significantly different from GOE distribution. Such a distribution should be expected for systems with presently considered symmetry properties whose classical dynamics is mixing. A more careful look at their continuity properties shows that they possess one common feature. As it can be easily seen, distributions (15)–(17) can be characterized by nonzero values for null spacing, or in other words by discontinuity of spacing distribution at null spacing indicating, characteristic for integrable systems, clustering of levels [4].

The correlation between a simple structure of the graph for all discussed here simple graphs and properties of obtained for them spacing distributions seems to be evident. It can be understood when properties of the propagator are taken into account. In the case of multiple connected spaces, it can be written as a sum over irreducible loops in the configuration space [17]:

$$K(x'',x',E) = \sum_{\alpha} \chi_{\alpha} \int \mathcal{D}[x(t)] e^{-(i/\hbar)S_{\alpha}[x(t)]}. \qquad (18)$$

In the general case, when explicit expression of formula (18) becomes very complicated [18], the levels with GOE like spacing distribution are obtained. However, in the case of some graphs, where parts of this sum are relatively simple, some levels which are poles of different parts of the sum (18) might be quantized according to the EBK rules. Below, we present obtained factorizations of spectral equations for several simple graphs. The possibility of performing such factorizations means that the spectra can be decomposed into several subspectra. As will be shown after the presentation of these examples, usually one part of obtained equations has zeros which are given by a very simple formula allowing to write corresponding energies in the form which resembles the EBK quantization condition.

First, we consider an eight shape graph. The numerator of the secular equation takes the form

$$\sin(kl_2)\cos(kl_1) - \sin(kl_2) + \sin(kl_1)\cos(kl_2) - \sin(kl_1) = 0 \qquad (19)$$

and the whole equation after the factorization of the numerator and simplification reads

$$\sin[k(l_1 + l_2)/2][\cos(kl_1/2)\cos(kl_2/2)]^{-1} = 0. \qquad (20)$$

Then for a loop and a bond connected to a vertex one has

TABLE I. Example of levels identification procedure for three-bond graph.

E_n	$(\alpha_1,\alpha_2,\alpha_3)$	E_n	$(\alpha_1,\alpha_2,\alpha_3)$
71.262645		71.285714	(0 0 1)
71.265460		71.289495	
71.266667	(0 0 1)	71.290952	(0 1 0)
71.270117		71.294511	
71.273678	(0 1 0)	71.295238	(0 0 1)
71.275561		71.297693	(1 0 0)
71.276190	(0 0 1)	71.299853	
71.276536	(1 0 0)	71.303880	
71.281395		71.304762	(0 0 1)
71.284638		71.308226	(0 1 0)

$$2\cos(kl_1)\cos(kl_2) - 2\cos(kl_1) - \sin(kl_1)\sin(kl_2) = 0 \tag{21}$$

and the numerator can be simplified to

$$2\sin(kl_2/2)[2\sin(kl_2/2)\cos(kl_1) + \sin(kl_1)\cos(kl_2/2)] = 0. \tag{22}$$

As the last but one example, we would like to take three-bond star graph

$$\sin(kl_1)\cos(kl_2)\cos(kl_3) + \cos(kl_1)\sin(kl_2)\cos(kl_3) + \cos(kl_1)\cos(kl_2)\sin(kl_3) = 0. \tag{23}$$

The secular equation for this system can also be written in the form

$$\{\sin[k(l_1+l_2+l_3)] + \sin(kl_1)\sin(kl_2)\sin(kl_3)\} \times [\sin(kl_1)\sin(kl_2)\sin(kl_3)]^{-1} = 0. \tag{24}$$

The second factor of this equation does not provide any new zeros. The first one, however, has a simple structure but it is not written as a product. Therefore, we have performed numerical investigations in order to check if the values of energy levels are somehow correlated with linear combinations of bond lengths. We have checked values of the wave vector written in the form

$$k = \pi \Big/ \left(\sum_{i=1}^{3} \alpha_i l_i\right) \quad \text{for } \alpha_i = -3,-2,\ldots,3 \tag{25}$$

for the three-bond star with bond lengths $l_1 = 148.492424$, $l_2 = 181.8653348$, $l_3 = 329.8672287$. In Table I, we present a small part of the obtained results. For 10 000 checked in this manner levels from the middle part of the obtained earlier spectrum consisting of 80 000 levels, we have been able to identify 4504 levels always obtaining $k = \pi/l_i$ where $i = 1,2,3$. The same procedure with the same accuracy when applied to the spectrum of graph having the shape of tetrahedron failed to identify any levels. Therefore, we conclude that, also in this system, it is possible to decompose the energy spectrum into several subspectra, among which several are very easy to compute. The case of graphs with disconnected bonds is trivial, since the eigenvalues are obtained from equations

$$\sin kl_i = 0, \quad \text{for all } i.$$

From presented calculations performed for several simple quantum graphs, we infer that for each of these graphs the existence of some important periodic orbit with length L which may be written as a linear combination of graph's lengths $L = \Sigma_i \alpha_i l_i$, may be postulated. Such an orbit may be then associated with a certain irreducible loop γ in the phase space of the graph. The action along this loop is given by

$$I_\gamma = \frac{1}{2\pi}\oint_L \hbar k_m dx = \frac{1}{2\pi}\hbar k_m L = \frac{1}{2\pi}\hbar\frac{2m\pi}{L}L = m\hbar. \tag{26}$$

In formula (26) we have used the fact that, for all our examples, the value of a wave vector k is given by zeros of function $\sin(kL/2)$ and, therefore, $k_m = 2m\pi/L$. Energies of these levels are therefore given by the usual EBK formula

$$E_{\mathbf{m}} = H(I_\gamma = m\hbar), \tag{27}$$

where H is a classical Hamiltonian and appropriate Maslov index equals zero. Our point is that the formula (27) holds only for certain energies, where the wavelength of the wave function distinguishes one closed loop in the phase space of the system considered, which gives the origin to the EBK quantization condition. Therefore, such a phenomenon has no classical analogy. Proposed explanation does not contradict the fact that the value of particular energy level should be obtained by means of performing an infinite summation over all possible closed orbits. Our procedure differs from the generic case only by the summation of paths belonging to this special irreducible loop in the phase space, which is possible due to the additive properties of the formula (18). Therefore, in this way we are able to obtain only a part of the energy spectrum.

From the above presented examples it can be inferred that even slight remnants of regular behavior of quantum systems, by which we mean the presence in their spectra of the EBK quantized energy levels are correlated with discontinuities of spacing of the systems considered. This observation can be generalized and written in a form of a corollary describing the connection between finite elements distributions and integrability of quantum systems.

Corollary. Discontinuity or singularity of the spacing distribution may be taken as a premise that in the spectrum of a quantum system exists a sequence of energy levels which are almost exactly quantized in accordance with the Einstein-Brillouin-Keller formula. The same may be expected if appropriate higher derivatives discontinuities appear for significant three- and four-point finite elements probability distributions.

As the EBK quantized levels, the levels whose energy is given by formula

$$E_{\mathbf{m}} = H[\mathbf{I} = (\mathbf{m} + \alpha/4)\hbar] \tag{28}$$

are considered (the EBK quantized levels are characteristic for quantum systems whose classical analogs are integrable). We assume that the case when superposition of several

Wignerian spacing probability distributions occurs (which can also produce spacing distribution discontinuity) can be ruled out due to the knowledge of symmetries or the classical phase space structure of the system. Distributions of three- and four-point finite elements will be discussed in the next section. We have not presented them before because analytical formulas of these statistical measures rather constitute mathematical apparatus of our corollary, than are the physical motivation of stating it. Their earlier discussion would only blur the main line of our reasoning.

We expect that there might be some systems, not natural but with specially fitted potentials, for which singularity or discontinuity of spacing distribution, or finite elements probability distributions higher derivatives discontinuities do not guarantee the existence of the regular levels sequence. The relationship between sequences of the EBK quantized levels and discontinuities of spacing distributions may also be questioned on the basis of the above mentioned results of Podolskiy and Narimanov [8]. However, although in spectra of the systems considered, levels which can be regarded as regular or in other words associated with KAM tori exist, these levels are not of interest for us. It happens because energies of the EBK quantized levels can be obtained from the values of quantized motion integrals characterizing one invariant tori in the phase space. On the other hand, chaos assisted tunneling occurs between distinct invariant tori [19]. Therefore, corrections to level energies must depend on both invariant tori's actions [20].

III. DISTRIBUTIONS OF THREE- AND FOUR-POINT FINITE ELEMENTS

In the papers by Duras and Sokalski [21] an observation was made that spacing is in general a two-point approximation of function $E(i)=E_i$ first derivative

$$s_i = \frac{\Delta^1 E(i)}{\Delta^1 i} = \frac{1}{i+1-i}(E_{i+1} - E_i). \tag{29}$$

The fact that the probability distribution of the differential quotient which can be treated as a finite element is used to characterize quantum systems properties with regard to their classical dynamics suggests that other finite elements of the function $E(i)$ might also be helpful in this matter. It is therefore interesting whether an analogy of spacing distributions discontinuities will also be encountered for these new distributions, especially in the context of obtaining some analytical results. A systematic discussion of the three-point statistical measures developed on the basis of finite elements is contained in [21]. Here we remind definitions of introduced there finite elements

$$\Delta^1_{a,\mathrm{fin}} E_{i+1} = \frac{1}{2(i+1-i)}(-3E_i + 4E_{i+1} - E_{i+2}), \tag{30}$$

$$\Delta^1_{s,\mathrm{fin}} E_{i+1} = \frac{1}{2(i+1-i)}(E_{i+2} - E_i), \tag{31}$$

$$\Delta^2 E_{i+1} = \frac{1}{(i+1-i)^2}(E_i + E_{i+2} - 2E_{i+1}), \tag{32}$$

which are three-point asymmetrical first differential quotient, three-point symmetrical differential quotient, and three-point symmetrical second differential quotient, respectively. Distributions of these quantities may be considered as supplementary characteristics of quantum chaos or integrability. To find formulas for the probability distributions of these quantities for chaotic systems, an ensemble consisting of 3×3 random matrices denoted from here as GOE(3) was used, i.e., $N=3$ was assumed in the Rozenzweig-Porter formula; cf. [1,2,22]. There can also be considered a standard probabilistic model of three level quantum integrable system spectrum with uncorrelated levels. Such a model will be denoted in the following as I(3). With the use of models GOE(3) and I(3) analytical formulas for the reminded above statistical measures were obtained [21]. After proper rescaling of the spectrum, these finite elements will be referred to with new names:

$$\Delta^1_{a,\mathrm{fin}} E_{i+1} \to X_{i+1}, \quad \Delta^1_{s,\mathrm{fin}} E_{i+1} \to Y_{i+1}, \quad \Delta^2 E_{i+1} \to Z_{i+1}. \tag{33}$$

Analytical formulas for these statistical measures were derived for ensembles consisting of only three energy levels. It is possible to expect that the situation encountered in this case should be similar to the one happening for the Wigner surmise which, although derived with the use of 2×2 matrices, stays in a good agreement with the results obtained in the infinite dimensional matrices limit. To check this issue, we have performed a computer experiment which proved predictions about good agreement of obtained analytical formulas and experimental histograms [23].

Then, we checked analytically, if there indeed were any regularities in analytical properties of the obtained probability density distributions for introduced finite elements. We begin the review of these results with formulas obtained for the chaotic model:

The dimensionless spacing

$$f_S^{\mathrm{GOE}(2)}(s) = \Theta(s)\frac{\pi}{2} s \exp\left(-\frac{\pi}{4}s^2\right), \tag{34}$$

$$f_S^{\mathrm{GOE}(2)}(s)\big|_{s\to 0^+} = \frac{81}{16\pi}s + O(s^3)$$

$$\Rightarrow f_S^{\mathrm{GOE}(2)}(s) \in \mathcal{C}^0(R),$$

$$f_S^{\mathrm{GOE}(3)}(s) = \Theta(s)\frac{729}{128\pi^2} s\left\{\left(s^2 - \frac{8\pi}{9}\right)\left[\mathrm{erf}\left(\frac{3s}{4\sqrt{\pi}}\right) - 1\right] + \frac{4}{3}s\exp\left(-\frac{9s^2}{16\pi}\right)\right\}\exp\left(-\frac{27s^2}{16\pi}\right), \tag{35}$$

$$f_S^{\mathrm{GOE}(3)}(s)\big|_{s\to 0^+} = \frac{81}{16\pi}s + O(s^3) \Rightarrow f_S^{\mathrm{GOE}(3)}(s) \in \mathcal{C}^0(R).$$

TABLE II. Smoothness classes of three-point finite elements distributions for chaotic and integrable models (fin. elem. stands for finite element and ~ denotes logical negation).

	GOE(3)				I(3)			
fin. elem.	t	x	y	z	t	x	y	z
class	$\mathcal{C}^0(R)$	$\mathcal{C}^3(R)$	$\mathcal{C}^3(R)$	$\mathcal{C}^\infty(R)$	$\sim\mathcal{C}^0(R)$	$\mathcal{C}^0(R)$	$\mathcal{C}^0(R)$	$\mathcal{C}^0(R)$

The dimensionless three-point asymmetrical first differential quotient

$$f_X^{\mathrm{GOE}(3)}(x) = \frac{81}{228488\pi^2}\left[910\sqrt{13}\pi x - 315\sqrt{13}x^3 - (390x^2 - 2704\pi)\exp\left(-\frac{441x^2}{52\pi}\right) - \sqrt{13}x(315x^2 - 910\pi)\mathrm{erf}\left(\frac{21x}{2\sqrt{13\pi}}\right)\right]\exp\left(-\frac{27x^2}{52\pi}\right), \quad x < 0, \tag{36}$$

$$f_X^{\mathrm{GOE}(3)}(x) = \frac{81}{228488\pi^2}\left[910\sqrt{13}\pi x - 315\sqrt{13}x^3 + (1638x^2 + 2704\pi)\exp\left(-\frac{25x^2}{52\pi}\right) + \sqrt{13}x(315x^2 - 910\pi)\mathrm{erf}\left(\frac{5x}{2\sqrt{13\pi}}\right)\right]\exp\left(-\frac{27x^2}{52\pi}\right), \quad x \geqslant 0, \tag{37}$$

and therefore

$$f_X^{\mathrm{GOE}(3)}(x)\big|_{x\to 0^+} - f_X^{\mathrm{GOE}(3)}(x)\big|_{x\to 0^-} = -\frac{27}{2\pi^3}x^4 + O(x^6) \Rightarrow f_X^{\mathrm{GOE}(3)}(x) \in \mathcal{C}^3(R).$$

The dimensionless three-point symmetrical first differential quotient

$$f_Y^{\mathrm{GOE}(3)}(y) = \Theta(y)\frac{81}{4\pi^2}y\left[6y\exp\left(-\frac{9y^2}{\pi}\right) + (9y^2 - 2\pi)\exp\left(-\frac{27y^2}{4\pi}\right)\mathrm{erf}\left(\frac{3y}{2\sqrt{\pi}}\right)\right], \tag{38}$$

$$f_Y^{\mathrm{GOE}(3)}(y)\big|_{y\to 0^+} = \frac{729}{2\pi^3}y^4 + O(y^6) \Rightarrow f_Y^{\mathrm{GOE}(3)}(y) \in \mathcal{C}^3(R).$$

The dimensionless three-point symmetrical second differential quotient

$$f_Z^{\mathrm{GOE}(3)}(z) = \frac{3}{2\pi}\exp\left(-\frac{9z^2}{4\pi}\right) \Rightarrow f_Z^{\mathrm{GOE}(3)}(z) \in \mathcal{C}^\infty(R) \tag{39}$$

and continue with the formulas for the integrable one.

The dimensionless spacing

$$f_S^{I(3)}(s) = \Theta(s)\exp(-s) \Rightarrow f_S^{I(3)}(s) \notin \mathcal{C}^0(R).$$

The dimensionless three-point asymmetrical first differential quotient

$$f_X^{I(3)}(x) = \begin{cases} \frac{1}{2}\exp(2x) & \text{for } x < 0, \\ \frac{1}{2}\exp\left(-\frac{2x}{3}\right) & \text{for } x \geqslant 0, \end{cases} \tag{40}$$

$$f_X^{I(3)}(x)\big|_{x\to 0^+} - f_X^{I(3)}(x)\big|_{x\to 0^-} = -\frac{4}{3}x + O(x^2) \Rightarrow f_X^{I(3)}(x) \in \mathcal{C}^0(R).$$

The dimensionless three-point symmetrical first differential quotient

$$f_Y^{I(3)}(y) = 4y\Theta(y)\exp(-2y), \tag{41}$$

$$f_Y^{I(3)}(y)\big|_{y\to 0^+} = 4y + O(y^2) \Rightarrow f_Y^{I(3)}(y) \in \mathcal{C}^0(R).$$

The dimensionless three-point symmetrical second differential quotient

$$f_Z^{I(3)}(z) = \frac{1}{2}\exp(-|z|) \Rightarrow f_Z^{I(3)}(z) \in \mathcal{C}^0(R).$$

Obtained results are gathered in Table II.

It may be observed that each measure, when calculated for the chaotic model, belongs to the class of smoother functions in comparison with class of the same measure calculated for the integrable model. In order to check whether these regularities preserve when more precise, i.e., built on the basis of more points expressions are considered, we have calculated analytical distributions of four-point finite elements. We have followed the method of Refs. [21] and have generalized presented there derivation in such a way that after this modification it can be more easily applied to statistical measures based on an arbitrary number of points. As an example of the application of this improved method, we have calculated distributions of five different four-point finite elements whose specific forms, appropriate for our application, were obtained from the definition of the finite element [24]

$$Z_1 = \Delta_{4,\mathrm{s}}^1 E_{5/2} = -\frac{1}{24}(E_4 - 27E_3 + 27E_2 - E_1), \tag{42}$$

$$W_1 = \Delta_{4,\mathrm{a}}^1 E_{3/2} = -\frac{1}{24}(E_4 - 3E_3 - 21E_2 + 23E_1), \tag{43}$$

$$Y_1 = \Delta^2_{4,\mathrm{s}} E_{5/2} = \frac{1}{2}(E_4 - E_3 - E_2 + E_1), \tag{44}$$

$$V_1 = \Delta^2_{4,\mathrm{a}} E_{3/2} = \frac{1}{2}(-E_4 + 5E_3 - 7E_2 + 3E_1), \tag{45}$$

$$U_1 = \Delta^3_{4,\mathrm{ps}} E_{5/2} = E_4 - 3E_3 + 3E_2 - E_1. \tag{46}$$

These are a four-point pseudosymmetric element approximating first derivative, a f-p. asymmetric element approximating first derivative (where f-p. stands for four-point), a f-p. symmetric element approximating second derivative, a f-p. asymmetric element approximating second derivative, and a f-p. pseudosymmetric element approximating third derivative, respectively. In the case of an integrable model, we have imposed the requirement that the mean level spacing should be equal to unity. Then, we have checked whether both side limits of these distributions derivatives are equal at zero, i.e., at the point where two parts of these distributions are joined together. In the case of the chaotic model, we were unable to calculate probability density distributions. We were, however, able to compare their Taylor expansions at both sides of potential discontinuity points. Actual calculations will be presented in a separate paper [25] and here only main results will be reviewed. We present full results for the integrable case whereas for the chaotic model only main conclusions will be summarized.

The four-point pseudosymmetric element approximating first derivative

$$f_{Z_1}(z_1)|_{D=1} = \begin{cases} \dfrac{16}{243D^2}(13D - 324z_1)\ \exp\left(\dfrac{24z_1}{D}\right)\Big|_{D=1}, & z_1 < 0, \\ \dfrac{208}{243D}\ \exp\left(-\dfrac{12z_1}{13D}\right)\Big|_{D=1}, & z_1 \geqslant 0, \end{cases} \tag{47}$$

$$\lim_{z_1\to 0^-} f^{-\prime}_{Z_1}(z_1) = -\frac{64}{81}, \quad \lim_{z_1\to 0^+} f^{+\prime}_{Z_1}(z_1) = -\frac{64}{81},$$

$$\lim_{z_1\to 0^-} f^{-\prime\prime}_{Z_1}(z_1) = -\frac{14336}{27}, \quad \lim_{z_1\to 0^+} f^{+\prime\prime}_{Z_1}(z_1) = \frac{256}{351}. \tag{48}$$

The four-point asymmetric element approximating first derivative

$$f_{W_1}(w_1)|_{D=1} = \begin{cases} \dfrac{1}{3D}\ \exp\left(\dfrac{24w_1}{D}\right)\Big|_{D=1}, & w_1 < 0, \\ \dfrac{1}{21D}\ \left[23\exp\left(-\dfrac{24w_1}{23D}\right) - 16\exp\left(-\dfrac{12w_1}{D}\right)\right]\Big|_{D=1}, & w_1 \geqslant 0, \end{cases} \tag{49}$$

$$\lim_{w_1\to 0^-} f^{-\prime}_{W_1}(w_1) = 8, \quad \lim_{w_1\to 0^+} f^{+\prime}_{W_1}(w_1) = 8,$$

$$\lim_{w_1\to 0^-} f^{-\prime\prime}_{W_1}(w_1) = 192, \quad \lim_{w_1\to 0^+} f^{+\prime\prime}_{W_1}(w_1) = -\frac{2496}{23}. \tag{50}$$

The four-point symmetric element approximating second derivative

$$f_{Y_1}(y_1)|_{D=1} = \begin{cases} \dfrac{1}{D}\ \exp\left(\dfrac{2y_1}{D}\right)\Big|_{D=1}, & y_1 < 0, \\ \dfrac{1}{D}\ \exp\left(-\dfrac{2y_1}{D}\right)\Big|_{D=1}, & y_1 \geqslant 0, \end{cases} \tag{51}$$

$$\lim_{y_1\to 0^-} f^{-\prime}_{Y_1}(y_1) = 2, \quad \lim_{y_1\to 0^+} f^{+\prime}_{Y_1}(y_1) = -2. \tag{52}$$

The four-point asymmetric element approximating the second derivative

$$f_{V_1}(v_1)|_{D=1} = \begin{cases} \dfrac{1}{35D}\ \left[15\exp\left(\dfrac{2v_1}{3D}\right) - 7\exp\left(\dfrac{2v_1}{D}\right)\right]\Big|_{D=1}, & v_1 < 0, \\ \dfrac{8}{35D}\ \exp\left(-\dfrac{v_1}{2D}\right)\Big|_{D=1}, & v_1 \geqslant 0, \end{cases} \tag{53}$$

$$\lim_{v_1\to 0^-} f^{-\prime}_{V_1}(v_1) = -\frac{4}{35}, \quad \lim_{v_1\to 0^+} f^{+\prime}_{V_1}(v_1) = -\frac{4}{35},$$

$$\lim_{v_1\to 0^-} f^{-\prime\prime}_{V_1}(v_1) = -\frac{64}{105}, \quad \lim_{v_1\to 0^+} f^{+\prime\prime}_{V_1}(v_1) = \frac{2}{35}. \tag{54}$$

The four-point pseudosymmetric element approximating the third derivative

TABLE III. Smoothness classes of four-point finite elements distributions for chaotic and integrable models (fin. elem. stands for finite element). In the case of the chaotic model $\mathcal{C}^3(R)$ means that the function belongs to at least $\mathcal{C}^3(R)$ class.

			GOE(4)		
fin. elem.	z	w	y	v	u
class	$\mathcal{C}^3(R)$	$\mathcal{C}^3(R)$	$\mathcal{C}^1(R)$	$\mathcal{C}^3(R)$	$\mathcal{C}^3(R)$
			I(4)		
fin. elem.	z	w	y	v	u
class	$\mathcal{C}^1(R)$	$\mathcal{C}^1(R)$	$\mathcal{C}^0(R)$	$\mathcal{C}^1(R)$	$\mathcal{C}^1(R)$

$$f_{U_1^I}(u_1)|_{D=1} = \begin{cases} \dfrac{2}{9D}\ \exp\left(\dfrac{u_1}{2D}\right)\Big|_{D=1}, & u_1 < 0, \\ \dfrac{1}{9D^2}\ \exp\left(-\dfrac{u_1}{D}\right)(3u_1+2D)\Big|_{D=1}, & u_1 \geqslant 0, \end{cases} \tag{55}$$

$$\lim_{u_1\to 0^-} f^{-\prime}_{U_1}(u_1) = \frac{1}{9}, \quad \lim_{u_1\to 0^+} f^{+\prime}_{U_1}(u_1) = \frac{1}{9},$$

$$\lim_{u_1\to 0^-} f^{-\prime\prime}_{U_1}(u_1) = \frac{1}{18}, \quad \lim_{u_1\to 0^+} f^{+\prime\prime}_{U_1}(u_1) = -\frac{4}{9}. \tag{56}$$

The results obtained for four-point finite elements are gathered in Table III. When four-point finite elements are taken into account in the chaotic case, all finite element distributions—except the symmetric approximation of the second derivative distribution, which has only the first derivative continuous (compare Table III), have all derivatives up to the third continuous. In the integrable case, there can be encountered a discontinuity of the first (52) or second derivatives (48), (50), (54), and (56) of finite elements distributions. The results, which are gathered in Table III, remain in an excellent agreement with the predictions of our corollary, i.e., distributions calculated for the chaotic and the integrable systems belong to different smoothness classes. It is also worth to notice that obtained analytical formulas for probability distributions, although derived for three- and four-level ensembles, may be applied to investigations of real spectra consisting of thousands of levels. Here an analogy with the wide range of applications of the Wigner surmise derived for an ensemble consisting of two interacting energy levels and Poissonian distribution which can be obtained for two randomly distributed noninteracting levels, modeling properties of regular systems spectra can be put forward. Moreover, an agreement between discussed analytical results and experimental histograms has been shown explicitly in [23] for three-point finite-element distributions and will be demonstrated for four-point finite elements in [25].

IV. CONCLUSIONS

We have presented several examples of different quantum systems with some remnants of classical integrability and described in the form of a corollary the relationship between properties of statistical measures and Hamiltonian systems' classical dynamics. We confirmed our observations by an investigation of the three-point and four-point finite-element distributions analytical properties. There may be raised a question that it is hard to judge from the histogram about discontinuity or singularity of a distribution. This difficulty can be, however, overcome by the increase of a number of energy levels taken into account. It is frequently possible due to the fact that the spectra can be often obtained numerically. Although our corollary is rather simple, it possesses a wide range of possible applications: from molecular chemistry, science of disordered materials through atomic and nuclear physics, to elementary particle physics and simple models of quantum mechanics. It may be used for any quantum system whose spectrum is available, and we are interested in the existence of the EBK quantized levels in such a system. It does not guarantee the existence of such levels but shows a clear direction in further research, and facilitates the distinction between the system in which one may expect such an interesting feature from other quantum systems. On the other hand, the fact that statistical measures constructed on the basis of finite elements can be used in the task of drawing an experimental distinction between systems with a different dynamics, can also be considered as an achievement. It can be regarded in this way because it extends the range of the application of this rather recently developed research apparatus.

[1] C. E. Porter, *Statistical Theory of Spectra: Fluctuations* (Academic Press, New York, London, 1965).
[2] T. Guhr, A. Müller-Groeling, and H. A. Weidenmüller, Phys. Rep. **229**, 189 (1998).
[3] O. Bohigas, M. J. Giannoni, and C. Schmit, Phys. Rev. Lett. **52**, 1 (1984).
[4] M. V. Berry and M. Tabor, Proc. R. Soc. London, Ser. A **356**, 375 (1977).
[5] C. B. Whan, Phys. Rev. E **55**, R3813 (1997).
[6] M. V. Berry and M. Robnik, J. Phys. A **17**, 2413 (1984).
[7] A. J. Lichtenberg and M. A. Lieberman, *Regular and Stochastic Motion* (Springer-Verlag, New York, 1983).
[8] V. A. Podolskiy and E. E. Narimanov, nlin.CD/0310034.
[9] J. Zakrzewski, K. Dupret, and D. Delande, Phys. Rev. Lett. **74**, 522 (1995).
[10] H. D. Meyer, J. Chem. Phys. **84**, 3147 (1986); O. Bohigas, S. Tomsovic, and D. Ullmo, Phys. Rep. **223**, 43 (1994).
[11] B. Eckhardt, G. Hose, and E. Pollak, Phys. Rev. A **39**, 3776 (1989).
[12] Th. W. Ruijgrok and K. Sokalski, Physica A **208**, 263 (1994).
[13] P. Sułkowski and K. Sokalski, Acta Phys. Pol. B **29**, 1943 (1998).
[14] T. Kottos and U. Smilansky, Phys. Rev. Lett. **79**, 4794 (1997); Ann. Phys. (N.Y.) **274**, 76 (1999).

[15] F. Barra and P Gaspard, J. Stat. Phys. **101**, 283 (2000).
[16] R. Blümel, Y. Dabaghian, and R. V. Jensen, Phys. Rev. E **65**, 046222 (2002).
[17] L. Schulman, Phys. Rev. **176**, 1558 (1968).
[18] A. G. M. Schmidt, B. K. Cheng, and M. G. E. da Luz, J. Phys. A **36**, L545 (2003).
[19] S. Tomsovic, J. Phys. A **31**, 9469 (1998).
[20] M. Wilkinson, Physica D **21**, 341 (1986).
[21] M. M. Duras and K. Sokalski, Phys. Rev. E **54**, 3142 (1996); Physica D **125**, 260 (1999).
[22] L. E. Reichl, *The Transition to Chaos In Conservative Classical Systems: Quantum Manifestations* (Springer-Verlag, New York, 1992).
[23] M. M. Duras, K. Sokalski, and P. Sułkowski, Acta Phys. Pol. B **28**, 1023 (1996).
[24] L. Collatz, *Numerische Behandlung von Differentialgleichungen* (Springer-Verlag, Berlin, 1955), Appendix, Table III.
[25] P. Sułkowski and K. Sokalski (in preparation).